06 Oct 1971

Correlation and Statistical Characteristics of Turbulence Fronts in the Wakes of Hypervelocity Bodies

R. H. Howell

J. L. French

CORRELATION AND STATISTICAL CHARACTERISTICS OF TURBULENCE FRONTS IN THE WAKES OF HYPERVELOCITY BODIES

Ronald H. Howell
University of Missouri-Rolla
Rolla, Missouri

James L. French
Sperry Rand Corporation
Huntsville, Alabama

ABSTRACT

Data on statistical wake turbulence of the far wake of sphere and cone models with velocities from 9,800 to 21,500 feet/second and range pressures from 50 to 120 mm Hg. are presented and analyzed. The measurement technique used is that of observing the turbulence edge position of the wake on schlieren films. The measured parameters are the wake width; edge roughness; auto-correlation function; microscale; e-fold, integral, and average eddy lengths; wake dissipation parameter; Kolmogoroff and energy containing wave number parameters; Lagrangian integral time scale parameter; Strouhal number; cross-correlation function; and wake edge velocity. The results of these measurements are compared with other investigators, as well as other methods of observing the character of the turbulence of the far wake. The present data shows reasonable agreement with that of other investigators using the same observation technique. However, there is a lack of agreement between the results from some of the methods of observation and/or measurement techniques. The severest criticism of the present method of observation is found to be the need for a meridional plane view correction factor along with the lack of a direct relation of the wake edge position to the internal turbulence structure.

INTRODUCTION

Hypervelocity bodies moving through the atmosphere generate wakes whose characteristic structures are influenced by the shape, size, and velocity of the bodies as well as the pressure and composition of the atmosphere. Knowledge of the discriminating characteristic structures and their relationship to the body shape, size, and velocity are essential for positive, early radar detection as well as for scientific analysis of the cause and effect in the wake structure. Recently,[1,2,3,4,5,6,7] aeroballistic ranges have been used to attempt to classify the effects of the basic body parameters on the turbulence structure of the wake behind subscale bodies. A variety of observation and/or measurement techniques have been incorporated in these investigations and one of the difficult problems is that of assessing the results of each technique and its relation to the results from the various other techniques.

The subject of the present investigation is the presentation and analysis of the statistical characteristics of schlieren observations of the turbulence edge of the far wake (2,000 - 20,000 body diameters) behind hypervelocity (10,000 - 22,000 fps) spheres and cones.

A simplified model of this type of wake flow indicates that in the near wake region (x/d < 1,000) the inviscid - viscid interactions play the dominant role in the formation of the wake structure while in the far wake, turbulent diffusion effects are dominant. The coupling of these regions is manifested in the nature of the turbulence which is present at the beginning of the far wake. This model of the far wake implies that in a region of the atmosphere through which a hypervelocity body has travelled the fluid is in turbulent motion having a distinct distribution of characteristic eddy sizes. The distribution of the characteristic eddy or vortex diameters depends on the characteristics of the near wake which in turn are contingent upon body size, body material, body geometry, velocity, angle of attack and ambient gas conditions. The origin of these vortices includes many sources such as vortex generation downstream of the body, boundary layer shock-wave interaction, and flow instabilities in the near wake.

The discriminating characteristics of far wakes which have been investigated using this type of observation include: i) standard deviation of the measured wake variable, ii) microscale and integral scale correlation lengths, iii) wake width growth, iv) periodicity of the measured wake variable, v) wake Strouhal Numbers, vi) power spectra function, vii) statistical nature (skewness, kurtosis) of the measured wake variable.

Several wake observables have been used to characterize the far wake structure. Fox and Rungaldier[6] used the signal from hot-film anemometers to obtain space and time correlations of the wake moving past the anemometers. A disadvantage of this method of observation is that the probe interference with the wake is not always negligible.

Sequential shadowgraphs were used by Schapker[1] and Uberoi and Kovasznay.[10] This method has the advantage of not interfering with the wake flow, however, it is restricted to rather dense atmospheres due to a loss in sensitivity as the density is reduced. French,[5] Clay, et al.,[8] and Herrmann, et al.[9] observed the wake by use of schlieren photographs. This method has an added advantage in that it can be used in lower density atmospheres than shadowgraphs because of its increased sensitivity. With the shadowgraph or schlieren method either wake edge position or film density can be used as the measured variable.

Electrostatic probes have been used by Heckman, et al.[3] and Slattery, et al.[4] to measure the electron or ion concentrations in the far wake. These concentrations can then be related to other wake characteristics. As with the hot-film anemometer, electrostatic probes can interfere with the wake structure itself.

Radar and microwave investigations of the far wake have been conducted by Zivanovic, et al.[11] and Lane[12] which are free of probe interference but introduce uncertainty as to the nature of the wake in relation to the measured reflected signals.

Other observable characteristics include sequential spark motion in the wake which yields a wake velocity distribution;[3] observation of the wake chemiluminescence;[13] interferometric observations;[7,14] electron beam traverse of wake; and holographic interferometric studies.[7]

All of the above measurement techniques possess certain advantages as well as some inherent disadvantages. The problem which persists is the relationship between the characteristics of the various observables and the relation of these characteristics to the initial generation of turbulence. The subject of this investigation is the presentation of additional wake data and the comparison of these results with other methods of measurement.

EXPERIMENTAL TECHNIQUE

1.-Range Description

The majority of the results reported herein were obtained from the von Karman Facility 1000-Feet Hypervelocity Range G located at the Arnold Engineering Development Center at Arnold Air Force Station, Tennessee. The basic components of this range are depicted in Fig. 1. The test vehicle launcher is a

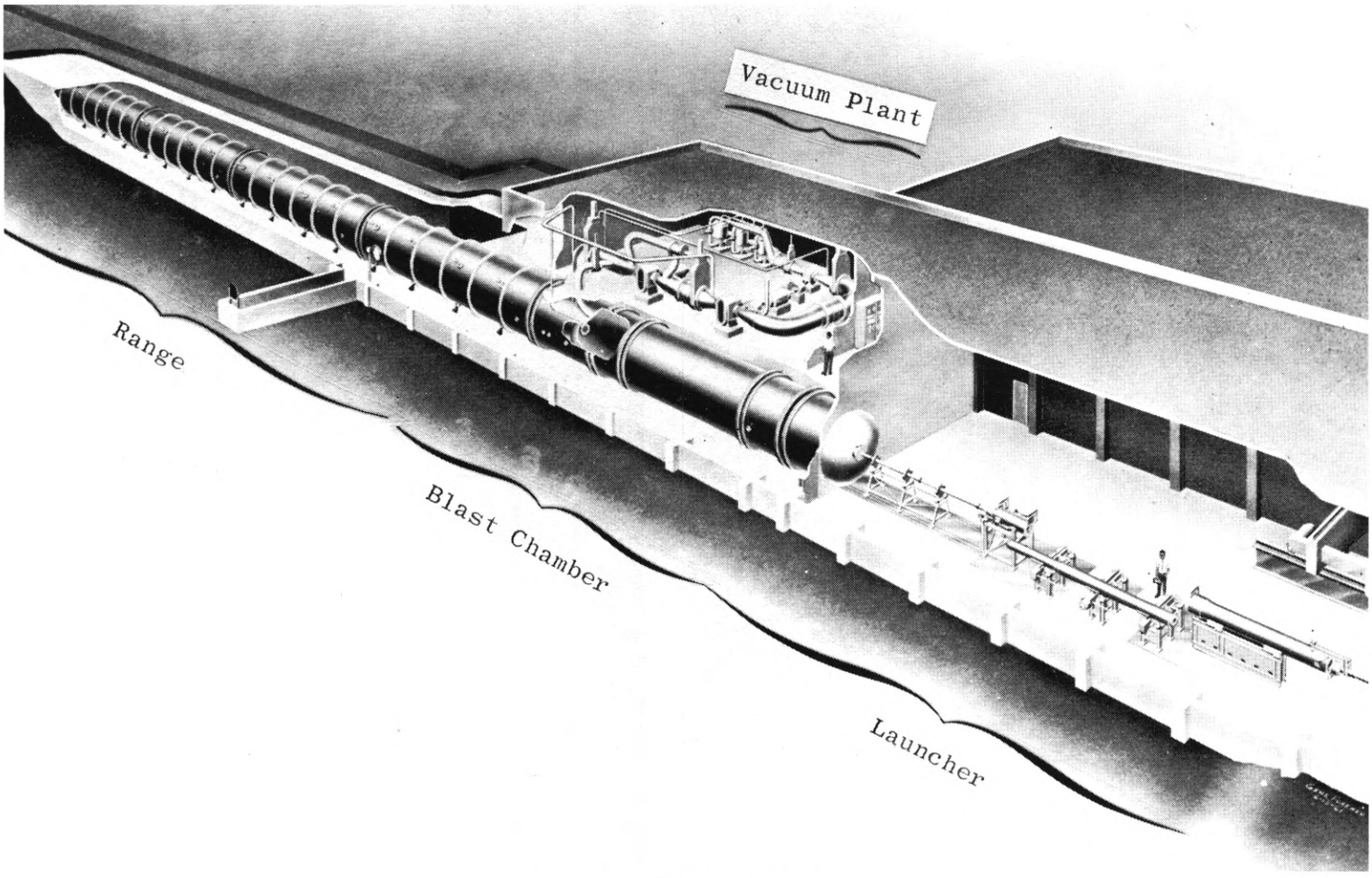

Fig. 1 VKF 1000-ft Hypervelocity Range G

two-stage powder-hydrogen gun connected to a 1000-foot long, 10-foot diameter test range with a controlled pressure (20 μHg to 1 atm.). The blast chamber in the range absorbs the muzzle blast and separates the model from the sabot. Cylinders, spheres, and cones with a major dimension of 0.5 inch to 2.5 inches made of plastic, steel, copper, or aluminum have been fired at velocities from 7,000 to 24,000 feet/second. A series of 43 shadow-graph stations allow position and attitude detection during the test.

The remainder of the data was obtained from the 100-foot Hypervelocity Range K at the Arnold Engineering Development Center. This range is a small scale version (pilot range) of Range G and has similar performance characteristics.

2.-Multiframe Schlieren Instrumentation

The primary instrumentation for the wake turbulence measurements was a high sensitivity, single-pass, schlieren system positioned 88.5 feet from the test range entrance. The system has a viewfield diameter of 30 inches and was operable in either single-frame or multi-frame modes. In the multiframe mode a multiflash Strobokin light source with a variable flashing frequency covering a range from 16 to 50,000 frames/second was used in conjunction with a high speed drum camera. With this system as many as 20 photographic frames were obtained. Examples of the multiframe schlieren pictures are shown in Fig. 2 for a 0.5-inch diameter sphere and for a 0.5-inch base diameter 10° cone.

3.-Measurement Technique and Procedure

The method which was used for analyzing the wake edge position in schlieren pictures was similar to that established by Schapker.[1] An image of the schlieren picture to be analyzed was magnified and reflected onto a film reader screen having two moveable perpendicular cross wires (Telereadex Type 29E manufactured by Benson-Lehner Corporation). The linearity accuracy was within 0.0028 inch in the plane of the magnified image. The output of the X-Y position of the wake edge was converted to punch card format which was finally analyzed using a Control Data Corporation 1604 computer.

Fig. 3 is a sketch of the geometry used in the measurement technique for the location of wake edge position. A reference line or mean wake axis was drawn near the center of the wake. The distance to the wake edge, y_u (upper outline) and y_L (lower outline), was measured perpendicular to the wake axis and repeated at a constant increment size ΔX. The pictures were read with a magnification of 20X and an increment size of 0.0667 inch. The sample length was 29 inches which generated 440 points on the upper profile and a like number on the lower profile.

At the upper profile, the y_u values were averaged according to a least squares method to find the best straight line through the points ($y_u' = a + bx$). Then, at any x, the deviation $\varepsilon_u = y_u - y_u'$ was calculated and from this ε_u ensemble all of the statistical parameters were determined. Similar calculations were made for the lower outline, and the resulting statistical parameters were averaged with those from the upper outline.

An analysis of the effect of a change of increment size on the wake parameters was given by French[5] and showed that a value of $\Delta X = 0.067$ inch could be used for all of the wake region. A value of $2\Delta X$ for increment size would yield a maximum error of 10% in λ in the very far wake and essentially no change in σ_ε.

The length of sample size was also analyzed by French[5] and he concluded, that just as in the case for the sample increment size, a change in sample length (to 22.5 inches, or 15 inches) can affect the microscale values, especially in the very far wake but has little effect on edge roughness or width. A sample length of 30 inches appears to be adequate out to 22,000 body diameters

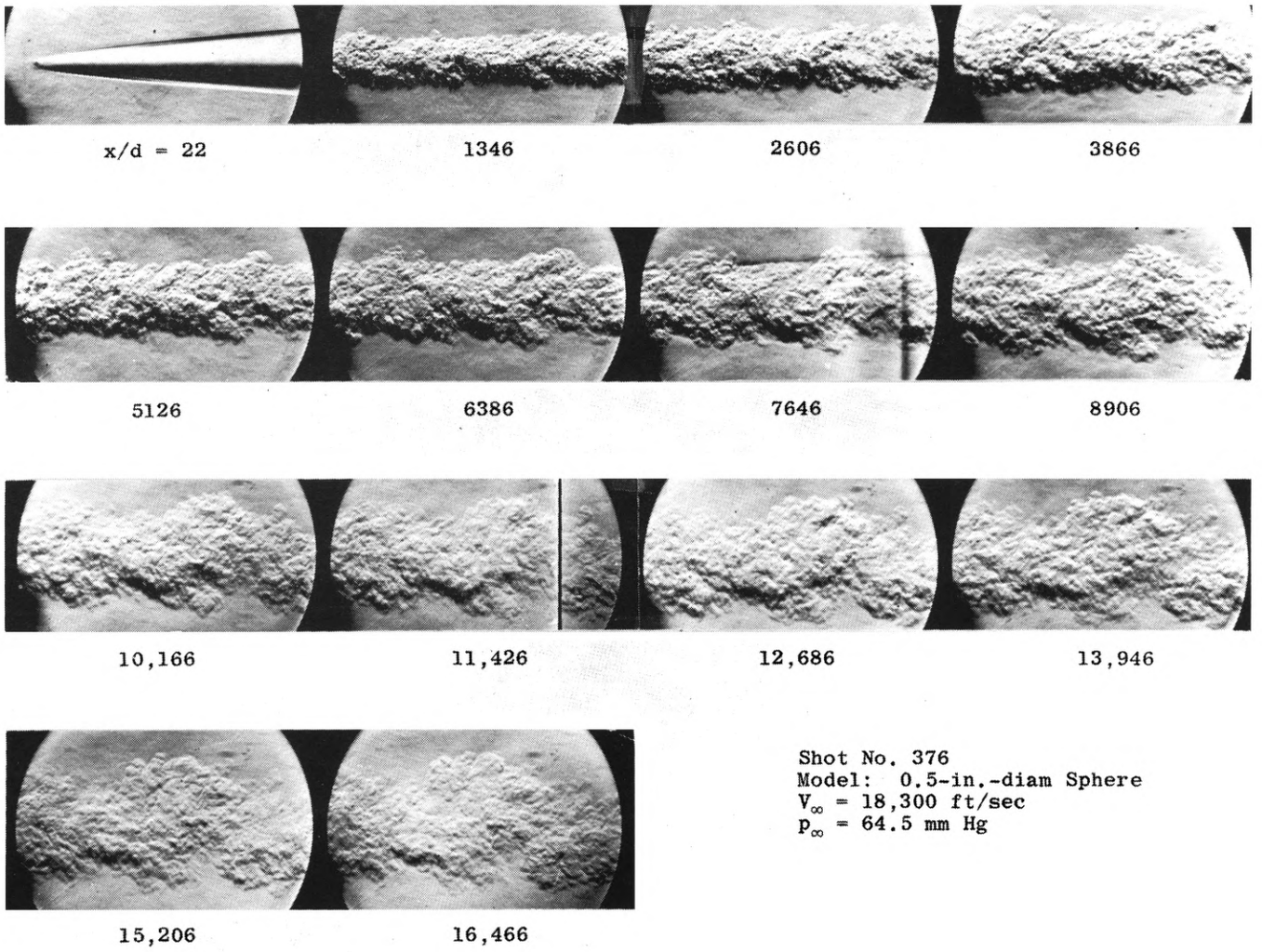

Fig. 2a. Multiframe Schlieren Photographs: Hypervelocity Sphere Wake

(for these models) and gives values which appear to be continuous in nature with a minimum of scatter (± 10%).

EXPERIMENTAL RESULTS

The conditions for the shots which were used for this analysis are given in Table 1. The angle of attack for the cone models was measured in the shadowgraph films and interpolated for the schlieren location. The data point symbols used for each shot are also given in order to avoid repetition of the conditions in each of the figures.

Data from other investigators have been used for comparison with the data presented in this analysis and these shot conditions are given in Table 2 along with their sources.

The dimensionless average wake width in the far wake is given in Fig. 4 for both the VKF shots and those of Schapker. In addition, the wake edge roughness σ_ε/d for both the VKF shots and those of Schapker[1] and Levensteins and Krumins[2] for both spheres and cones is given in Fig. 5.

From the basic measurements of the wake edge position statistical analyses were performed in order to find the statistical nature of the sample of measurements and to relate the wake edge position to typical turbulence characteristics.

DISCUSSION OF RESULTS

1.-Wake Width

The results given in Fig. 4 for the wake width of several of the sphere shots (606, 610, 624, 376) with identical size, velocity, and pressure verify that results from this type of wake observation and measurement technique are repeatable with a minimum of data scatter. In addition, it can be seen that the wake generated by cones moving at similar velocities and at the same pressure are smaller than those of spheres at corresponding x/d positions (shots 385, 422, 396). Also, there is no apparent effect on the wake width generated by cones due to differences in the angle of attack (up to 8.4°). For larger cone half-angles (shot Nos. 385, 396, 753) the wake width appears to be larger and growing at a greater rate. It is evident that the data obtained in the VKF ranges exhibit reasonable agreement with those of other investigations such as Schapker[1] and Levensteins and Krumins.[2]

It should be noted that if the wake width were plotted in terms of the drag diameter ($\omega/\sqrt{C_D A}$ versus $x/\sqrt{C_D A}$) that the curves for the cone and sphere collapse to a single curve for large values of $x/\sqrt{C_D A}$. Examples of this behavior are given by Slattery, Clay, and Herrmann.[4]

2.-Standard Deviation of Wake Edge

The standard deviation σ_ε of the wake edge position is defined by Eq. 1:

$$\sigma_\varepsilon = \left[\frac{1}{\ell} \int_0^\ell \varepsilon^2(x)\,dx \right]^{1/2} \qquad (1)$$

and represents an indication of the roughness of the wake edge. The wake edge roughness increases with distance along the wake and exhibits some scatter as shown in Fig. 5. There is exceptional agreement between this data and that of Schapker[1] and Levensteins and Krumins.[2]

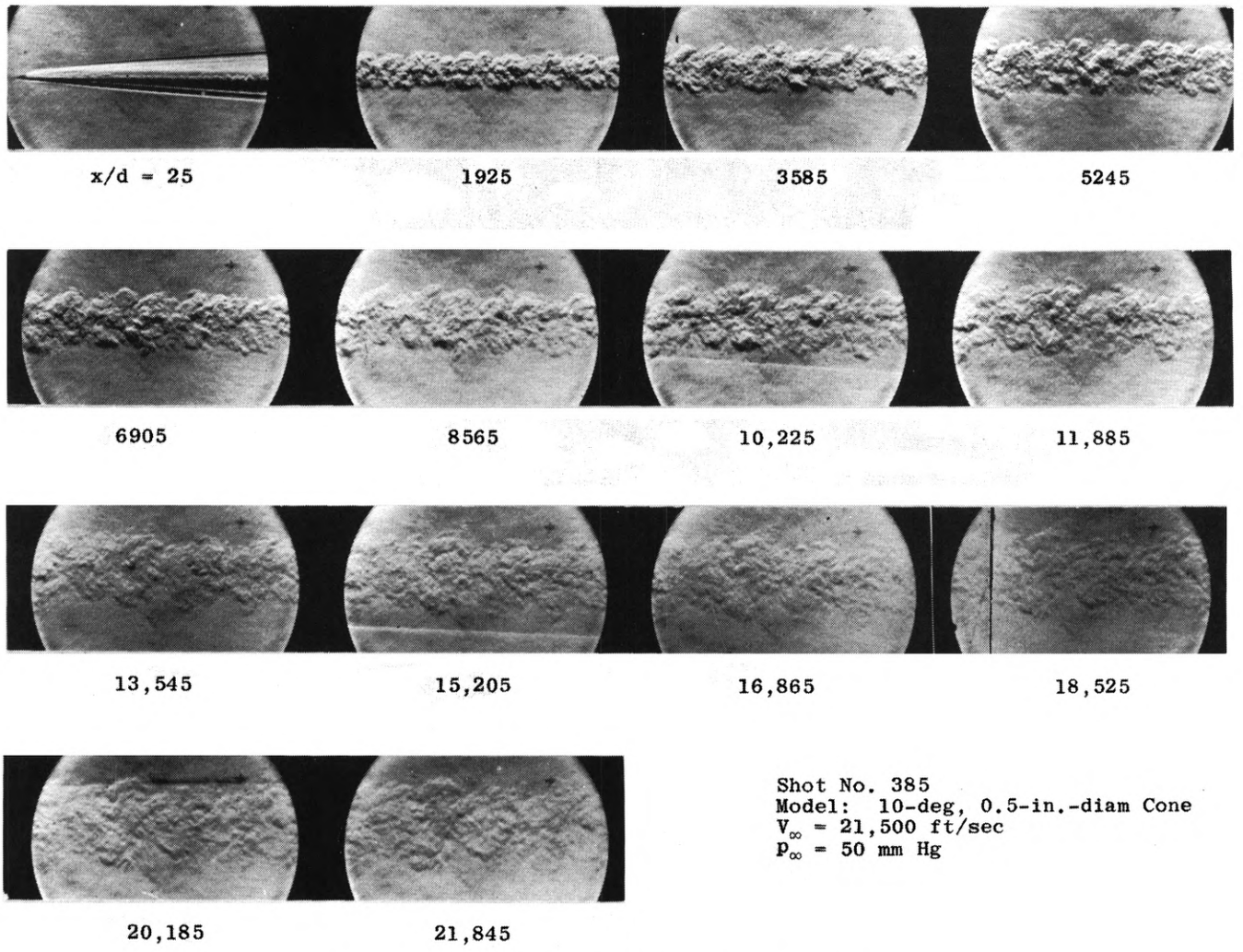

Fig. 2b. Multiframe Schlieren Photographs: Hypervelocity Cone Wake

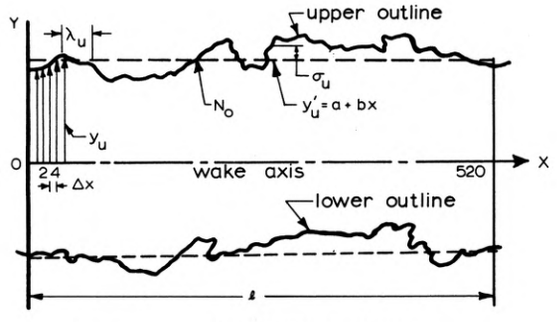

Fig. 3 Wake Outline Nomenclature

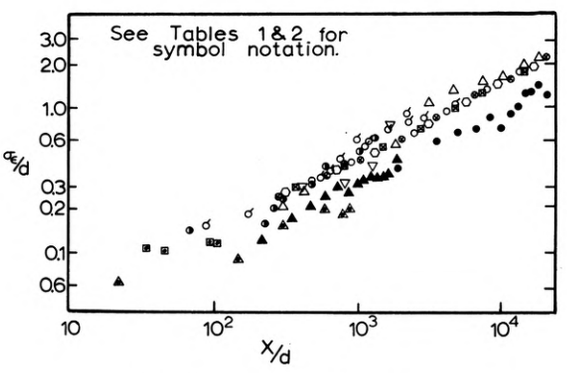

Fig. 5 Wake Edge Roughness

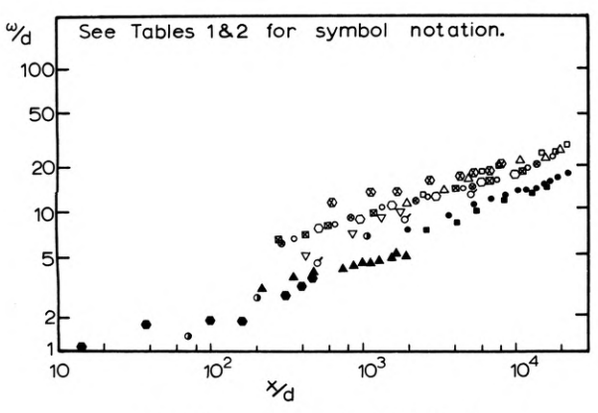

Fig. 4 Growth of Wake Width

There appears to be no discernible effect in σ_ε/d due to pressure or velocity differences. However, the edge roughness is always greater for spheres than for cones at the same axial locations. At this point it is not clear whether Re_∞, M_∞, or ambient atmospheric properties are more important in determining wake edge fluctuations. To determine this, however, would require a more systematic program of controlled shot conditions.

As with wake width, there is no appreciable change in edge roughness for changes in cone half-angles.

There is a decrease in the rate of change of the roughness for some of the bodies. This could be due to a difference in the character of the turbulence which is initially generated near the body and eventually moves to the wake edge through turbulent diffusion.

TABLE 1 VKF SHOT CONDITIONS

Shot No.	Model	d in.	P_∞ mmHg	V_∞ ft/sec	Angle of Attack	M_∞	$Re_\infty \times 10^{-5}$	Material	Symbol
376	sphere	0.500	64.5	18,300	----	16.3	3.86	Cu	○
379	sphere	0.375	36.6	18,380	----	16.3	1.64	Cu-Al	□
381	sphere	0.500	120.0	20,660	----	18.3	8.06	Cu	△
606	sphere	0.500	64.2	18,310	----	16.3	3.85	Cu	⬡
610	sphere	0.500	64.5	18,335	----	16.3	3.86	Cu	⊗
624	sphere	0.500	64.2	18,498	----	16.4	3.9	Cu	⊠
1098	sphere	0.438	600.0	9,800	----	8.7	19.4	Fe	▽
1379	sphere	0.250	50.0	21,900	----	18.6	1.71	Al	⊗
385	10°-cone	0.500	50.0	21,500	6.1°	19	3.5	---	●
422	6°-cone	0.400	78.0	21,500	0.11°	19	4.4	---	▲
396	10°-cone	0.500	52.0	21,000	1.87°	18.6	3.58	---	■
753	10°-cone	1.00	49.2	10,160	4.4°	9.0	3.25	---	⬢

TABLE 2. SHOT RESULTS FROM OTHER INVESTIGATORS

Model	d in	P_∞ mm Hg	V_∞ ft/sec	M_∞	Re_∞ x10^{-5}	Reference	Symbol
sphere	0.125	760	3600	3.2	2.5	1	♂
sphere	0.25	760	5300	4.7	7.1	1	◑
9° cone	0.87	200	11000	10.3	13.0	2	⧋
9° cone	0.25	260	12000	10.6	5.17	2	◬
8° cone	0.40	270	14300	12.6	11.0	1	⧈
24° - cone	0.37	200	-----	10	4.88	2	⊏
sphere	0.19	40	18400	16.3	-----	2	⊛

Some of the scatter and deviation can be attributed to the method of obtaining the edge position from the schlieren photographs. If the wake axis (see Fig. 3) is located incorrectly, changes in wake edge position can show greater deviations on one side of the wake than the other due to the differences in the absolute distances.

In addition to this effect, some differences in wake edge roughness can be attributed to transition effects in the boundary layer on the body as well as body size effects on the transition location. In an experimental study of transition in the wake of cones,[16] it has been suggested that for $Re_\infty < 2 \times 10^5$ distance to transition is dependent upon the absolute size of the model. If such effects exist in transition measurements, it is reasonable to expect that the subsequent turbulent structure may be size dependent. This suggests the desirability of separately studying size and the usual dimensionless parameters.

The moment coefficient of skewness for the wake edge data defined in Eq. 2:

$$\frac{\sum_{j=1}^{N} (y_j - \bar{y})^3}{N\sigma_\varepsilon^3} \qquad (2)$$

is shown in Fig. 6 for several of the sphere shots (376, 379, 381). These values are the average absolute values for the upper and lower wake profiles.

This coefficient assigns a numerical value for the degree of skewness of the distribution from the mean value. For a Gaussian distribution, the moment coefficient of skewness is zero. From these results it is apparent that the data is skewed to the positive (as expected for a growing wake) and that it exhibits a periodic nature along the wake axis.

The moment coefficient of kurtosis defined in Eq. 3:

$$\frac{\sum_{j=1}^{N} (y_j - \bar{y})^4}{N\sigma_\varepsilon^4} \qquad (3)$$

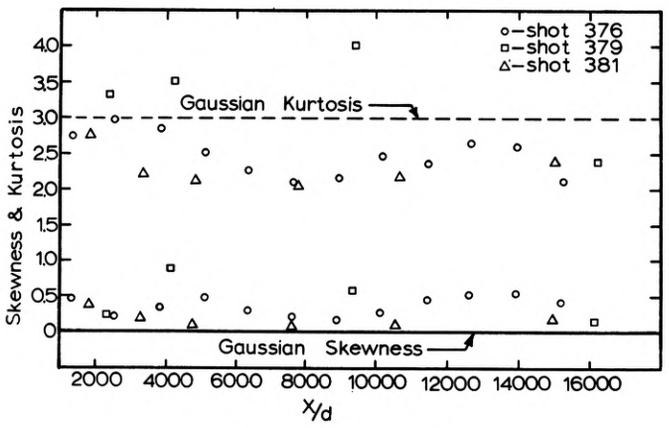

Fig. 6 Skewness and Kurtosis of Wake Edge Distribution

is the degree of peakedness of a distribution which has a value of three for a Gaussian distribution. The kurtosis coefficient is also shown in Fig. 6 for the same sphere shots (averages of upper and lower edges). Again, the average kurtosis indicates that the distribution is non-Gaussian and the coefficient appears to be a damped periodic function.

3.-Autocorrelation Function and Correlation Lengths

A sample of the normalized autocorrelation function of the deviation of the wake edge position for a 0.375-inch diameter sphere (shot 379) is presented in Fig. 7 as a function of the correlation lag increment K. The normalized autocorrelation function is defined as

$$RE(\xi) = \frac{Q_\varepsilon(\xi)}{Q_\varepsilon(0)} \qquad (4)$$

where

$$Q_\varepsilon(\xi) = \frac{1}{\ell-\xi} \int_0^{\ell-\xi} \varepsilon(x)\ \varepsilon(x+\xi)dx$$

and ξ = correlation lag distance = $K\Delta X$. The results presented in Fig. 7 were obtained by numerically integrating Eq. 4 with ΔX = 0.0667 inch.

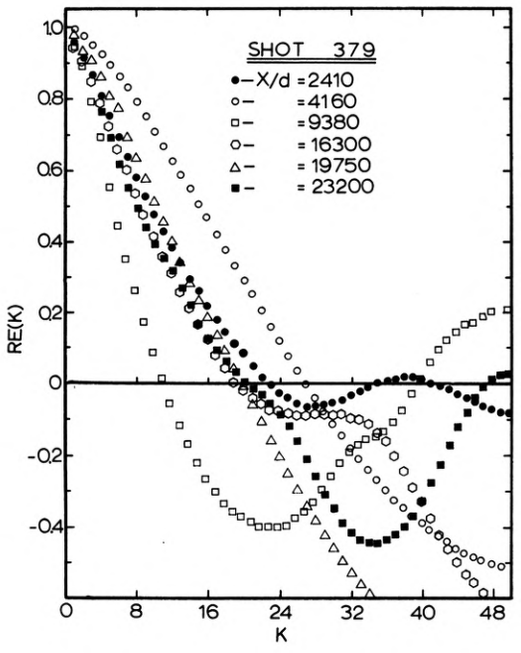

Fig. 7 Normalized Autocorrelation Function

For isotropic and homogeneous turbulence the correlation function is a symmetrical function and varies between plus and minus one. When the autocorrelation function has a value of near plus one there is a strong linear relationship between $\varepsilon(X)$ and $\varepsilon(X+\xi)$. Therefore the correlation lag distance, ξ, represents the distance over which the deviation is linearly related. The further away from plus one the smaller is the tendency for a linear relation. However, there might be some other relation between the deviations besides a linear one. The autocorrelation function as defined here only indicates the tendency for a linear relationship.

As expected, the autocorrelation function decreases toward zero as the correlation lag increases. Very little can be said about the shape of the autocorrelation function since it depends upon the structure of the turbulence. It may decrease beyond zero to a significantly negative value or oscillate about zero. There is no apparent similarity or pattern in any of the correlation functions since at some locations it approaches zero in an oscillatory manner (Fig. 7: x/d = 2,410; 23,200) while at others it drops well below zero (Fig. 7: x/d = 16,300; 19,750), and shows no evidence of oscillation.

The true significance of the autocorrelation function is derived from the various correlation lengths which can be obtained from the function itself. Near ξ = 0, a parabola can be used to describe the shape of the curve and the intersection of this parabola with the ξ - axis is used to define the microscale correlation length, λ.

The microscale length is an indication of the dimension of the smallest eddies "on the average" which cause a change in the local velocity. λ is defined by:

$$\lambda = \left(- \frac{2}{\left(\frac{\partial^2 RE(\xi)}{\partial \xi^2} \right)_{\xi=o}} \right)^{1/2} \tag{5}$$

The e-fold length, Le, is the correlation lag ξ where $RE(\xi)$ reduces to a value of 1/e. This length is a convenient well defined point on the autocorrelation curve (if it is an ordinary function) and it is generally accepted as a measure of the longest linear correlation distance between the deviation at two points in the flow field sample.

The integral correlation length is defined as:

$$L_I = \int_0^{\xi_{max}} RE(\xi)d\xi \tag{6}$$

and is representative of the longest correlation distance between two points in the flow field sample. This definition however is ambiguous when a periodic function of $RE(\xi)$ exists yielding the possibility of negative values for L_I. For a periodic correlation function, a finite domain should be specified for the integration limits.

The e-fold and integral length are representative of the size of vortices which contain the majority of the kinetic energy in the turbulent fluid and which in turn degenerate into small scale eddies (measured by λ), which eventually dissipate the energy in the wake. Because of this mechanism of decay the correlation lengths should become approximately equal in the far wake.

Representative values of the microscale length are given in Fig. 8 for several sphere and cone shots as well as some of the values from other investigators.

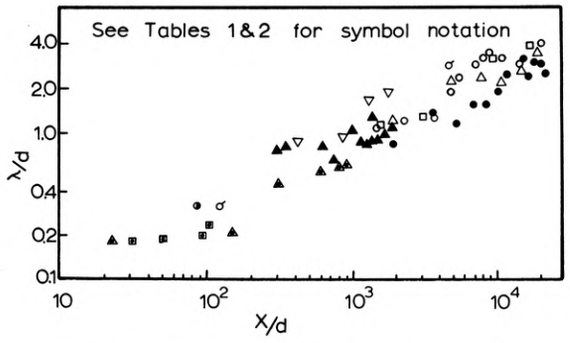

Fig. 8 Microscale Correlation Length

In order to evaluate the microscale correlation length (defined by Eq. 5) a parabola must be fitted to the autocorrelation functions at ξ = 0. Since this would be an inexact method for evaluating λ, an approximate method was used. Corrsin and Kistler[17] developed an approximate method which uses the number of zero crossings of the wake edge. Their method, which assumes a Gaussian distribution for the deviations, can introduce some inaccuracies into these values for non-Gaussian distributions of the wake edge deviations. Intermittency calculations were made in order to establish the Gaussian nature of the wake edge deviations.[5]

The intermittency factor which is defined to be the percentage of the time that the fluid at a fixed location is within the turbulent wake is given by:

$$\int_y^\infty P_f(y')dy'$$

where $P_f(y')$ denotes the probability density of the front. The intermittency factors were evaluated[5] for much of the wake edge data. It was evident from these results that the intermittency factor followed a Gaussian-type distribution for many different shots at various positions in the far wake. These results support the use of the approximate method given by Corrsin and Kistler[17] for evaluating the microscale length.

The cone appears to exhibit a lower value of λ/d than the spheres which might be expected for sharp bodies in comparison to blunt bodies. The dimensionless microscale length, λ/d, increases with increasing x/d.

In Fig. 9 are representative values of the e-fold length and the integral length (integrated irrespective of oscillations) for several spheres (shots 376, 379, 381). There is some dispersion of the results. However, the trend of the results is similar to that for the microscale length. The magnitudes of the e-fold length and L_I are slightly higher than λ but both are nearly equal in the very far wake.

An additional correlation length has been calculated and is shown in Fig. 10. This length, $\bar{x}$, is the average axial distance between peaks in the wake edge. This distance is indicative of the average vortex size in the wake and its order of magnitude is the same as that of the body, as expected. There appears to be an oscillatory behavior of $\bar{x}$ in the wake which shows an increasing wavelength in the axial direction with a decrease in amplitude. The $\bar{x}$ length appears to be a reasonable correlation length and has the advantage of not requiring the calculation of RE(ξ).

Various correlation lengths from various instrumentation systems have been compared in Fig. 11. From this comparison it is apparent that at most positions in the wake there is an order of magnitude difference in the results from various means of measuring correlation lengths. This amount of deviation should be resolved by further investigation of the far wake as well as more detailed analyses of the measurement techniques involved.

4.-Turbulence Quantities

Several of the relevant turbulence characteristics have been calculated in order to relate the wake edge statistics to the internal turbulence of the wake. The relations between front statistics and the internal turbulence structure are inherently approximate, since the wake edge characteristics

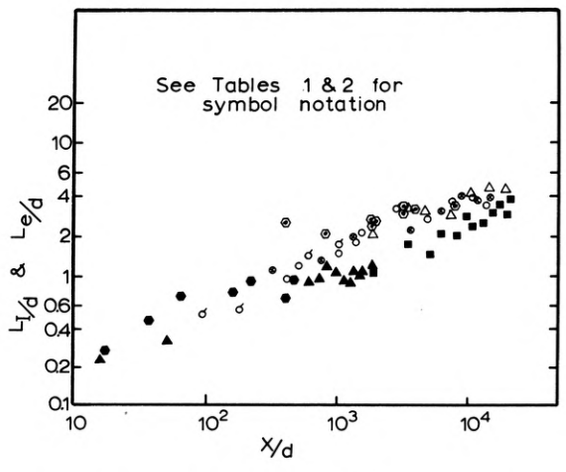

Fig. 9 Integral and E-fold Correlation Lengths

are only boundary measurements. The details of the derivations of these relations are given by Schapker.[1]

The dissipation parameter, which is the entire left-hand side of Eq. 7, was related to wake edge properties by Schapker.[1] Values for the dissipation

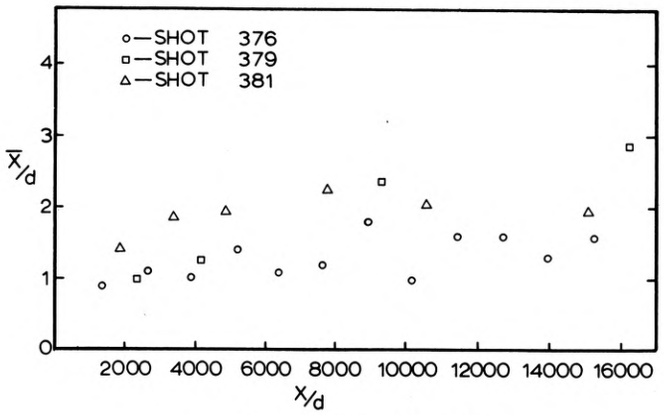

Fig. 10 Average Edge Eddy Size

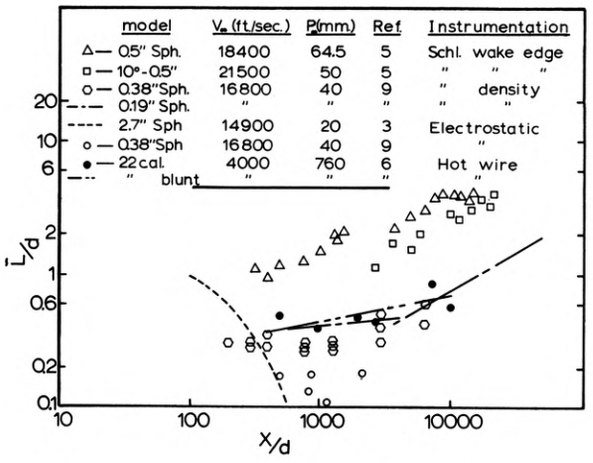

Fig. 11 Comparison of Correlation Length Measurements

parameter:

$$\frac{\phi d}{V_\infty} \mathrm{Re}^{1/2} \left(\frac{T_f}{T}\right)^{-0.8} \beta^{-5/2} = 1.4 \frac{\sigma_\varepsilon}{d} \left(\frac{\lambda}{d}\right)^{-2} \eta^{-1/2} \qquad (7)$$

for several sphere shots (376, 379, 381) are given in Fig. 12. It can be observed that the incompressible dissipation rate is approached in the far wake and that the actual dissipation is less than the predicted incompressible dissipation out to about 10,000 body diameters. The dissipation parameter relates the temperature fluctuations at the front edge and the velocity of the front edge to the edge position statistics.

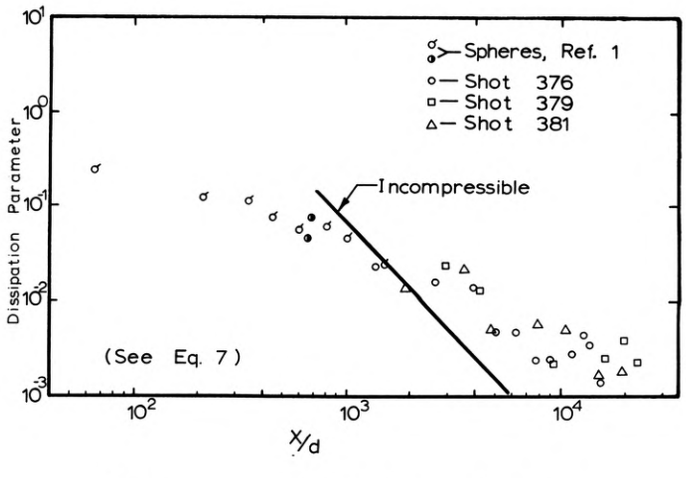

Fig. 12 Turbulence Dissipation in the Far Wake

Fig. 13 contains the data for the Kolmogoroff wave number parameter (left hand side of Eq. 8) and its predicted relation to the wake edge:

$$K_d d(V_\infty \frac{\rho_\infty}{\rho_o} d)^{-5/8} (\frac{T_\infty}{T_o})(\frac{T_f}{T_\infty}) = 5.12 \times 10^3 (\frac{\sigma_\varepsilon}{d})(\frac{\lambda}{d})^{-1/2} \eta^{-1/8} \quad (8)$$

position statistics as given by Schapker[1] as well as the energy containing wave-number parameter (left hand side of Eq. 9):

$$K_e d(V_\infty \frac{\rho_\infty}{\rho_o} d)^{1/8} (\frac{T_f}{T_\infty})^{-0.2} = \frac{0.337}{C_D} (\frac{\lambda}{d})^{-1/2} (\frac{\sigma_\varepsilon}{d})^{-5/4} \eta^{5/8} \quad (9)$$

The Kolmogoroff wave number indicates the frequency of the small scale energy waves where the dissipation occurs while the energy containing wave number indicates the frequency of the large scale vortices which contain the

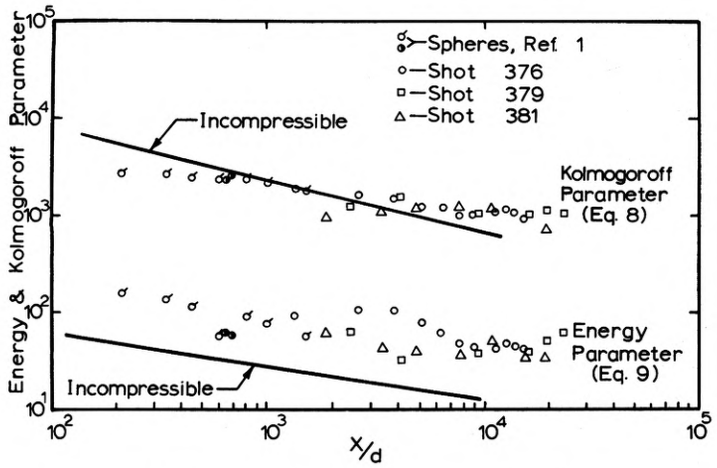

Fig. 13 Wave Number Parameters in Far Wake

majority of the kinetic energy. Reasonable agreement exists between the present data and the accepted relation from incompressible turbulence theory. These parameters provide the link between the edge turbulence, temperature fluctuations, and internal turbulence. These relations can be made on an empirical basis using measurements such as those presented by Demetriades.[18]

The Lagrangian integral time scale parameter [left hand side of Eq. 10] and its predicted variation[1] is presented in Fig. 14:

$$\frac{V_\infty L_\tau}{d} (\frac{\nu/\nu_\infty}{Re_\infty})^{1/4} \beta^{-3/4} = 0.6 (\frac{\sigma_\varepsilon}{d})^{1/2} (\frac{\lambda}{d}) \eta^{-1/4} \quad (10)$$

The Lagrangian integral time scale is representative of the longest time during which the fluid particles remain correlated. This parameter again relates the edge turbulence to the internal correlation function and the temperature intensity (on an empirical basis).

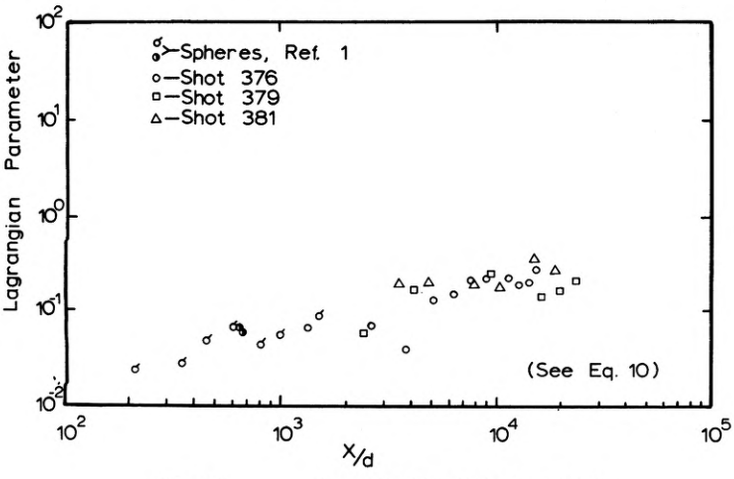

Fig. 14 Lagrangian Time Scale in Far Wake

Most of these turbulence quantities are reasonably well represented by their incompressible expressions, however, better empirical expressions can be obtained from the present results. Even so, further experiments and calculations for cones and other size spheres should be made before obtaining general empirical equations.

5.-Strouhal Number

The Strouhal number, N_{st}, for the wake has been calculated and is shown in Fig. 15:

$$N_{st} = \frac{\text{frequency} \times \sqrt{C_D A/2\pi}}{\text{velocity}} \quad (11)$$

N_{st} is a characteristic of the large scale motion in the wake. Two methods of calculation were used in computing N_{st}. The first used only vortices with

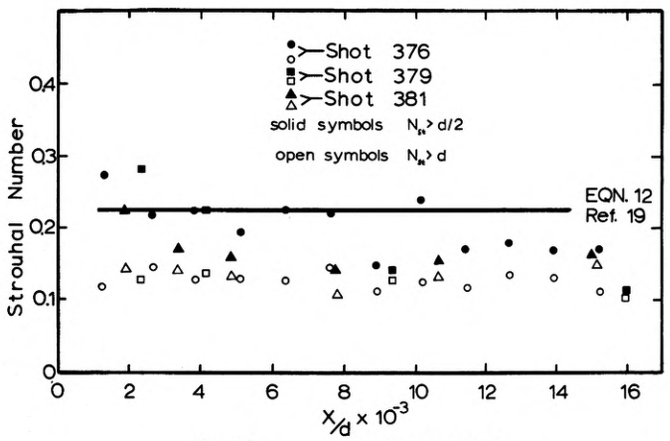

Fig. 15 Wake Strouhal Number

a diameter greater than the radius of the sphere and the second method used only vortices with a diameter greater than twice the radius of the sphere.[19]

The empirical expression for N_{st} given by Goldburg, et al.[20] is:

$$N_{st} = 0.229 (1 - \frac{1820}{Re_\theta}) \quad (12)$$

is in reasonable agreement with the present data. Again, after about 10,000 body diameters the Strouhal number appears to be constant as did the correlation lengths. This behavior of the Strouhal number is additional evidence of the periodic nature of the far wake.

6.-Cross-Correlation Calculations

The concept of the correlational function can be expanded to show the relationship between the deviation at one station (x/d position) and that at some other station. The cross-correlation function is defined as:

$$QC_{IJ}(\xi) = \frac{1}{\ell-\xi} \int_0^{\ell-\xi} \varepsilon_I(\xi)\varepsilon_J(x+\xi)dx \quad (13)$$

or in the normalized form as:

$$RC_{IJ}(\xi) = \frac{QC_{IJ}(\xi)}{QC_I(0)QC_J(0)} \quad (14)$$

The cross-correlations have been calculated for each station in the upper and lower edges separately for several shots (391, 379, 376). From the shift of the peak position of these functions the convection velocity at the edge of the wake can be estimated for each shot. The change in the peak value of the cross correlation function is a measure of the decay of the wake flow field.

The results from the wake edge velocity calculations are given in Fig. 16 along with measurements from other investigators. There is moderate agreement between the present data and another method of measurement (sequential spark) even though there is a great deal of dispersion in the far wake calculations.

Fig. 17 demonstrates the decay of the wake flow field. The ordinate is the maximum cross-correlation function and the abscissa is x/d. This comparison indicates that as the wake velocity decreases (Fig. 16), there is a lesser amount of decay. This behavior is indicative of an asymptotic type of wake decay, decreasing as x/d increases.

7.-Discussion of Method of Observation

One of the severest criticisms of this method of wake analysis is that the edge of the wake is not observed in a single plane but in a segment of the wake. This type of observation injects some bias into the statistical representation of the wake edge. This partiality for the maximum wake edge would tend to make the "average wake" larger than it actually is. The geometry of this concept is shown in Fig. 18. Schapker[1] showed that approximately seventy-five per cent of the outline points arise from actual occurrences within a ±30° segment centered about the meridional wake plane.

CONCLUSIONS

The important conclusions reached as a result of this investigation are:

i) On the basis of limited data, the turbulent wake width was found to increase with an increase in cone angle, and the wake widths for spheres were generally greater than for cones.

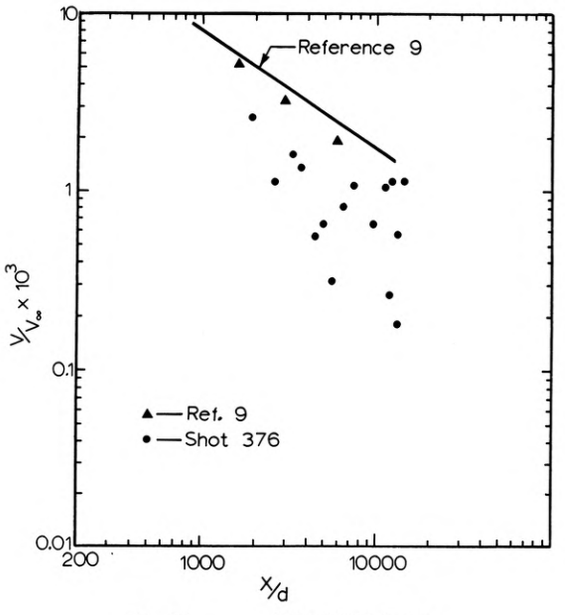

Fig. 16 Wake Edge Velocity

ii) The most reliable correlation lengths are the microscale length, e-fold length, and the average vortex size.

iii) Cross-correlation lengths yield a convection velocity for the wake edge and a wake decay measurement.

iv) Empirical relations between edge characteristics and internal turbulence structure can be formulated.

v) The readings of the wake edge obtained from the schlieren negatives should be corrected to obtain the meridional plane view.

vi) The wake edge position distribution appears to be non-Gaussian at some locations.

vii) Periodicity exists in the wake edge structure in some of the calculated quantities.

viii) The correlation lengths from several different measurement systems have been found to be quite similar.

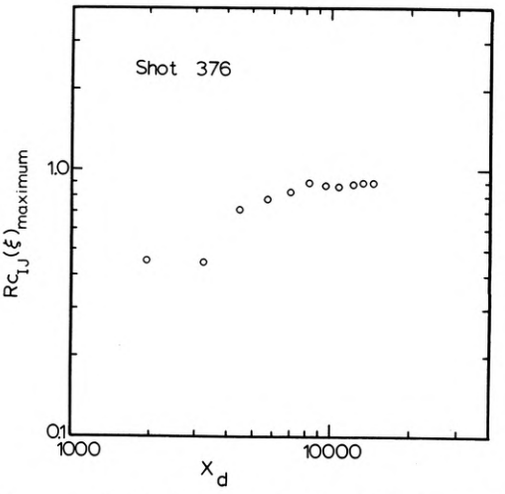

Fig. 17 Distribution of Maximum Value of the Normalized Cross-Correlation Function

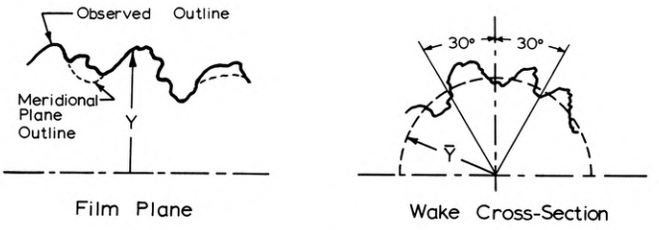

Fig. 18 Film-Plane Edge Geometry

ACKNOWLEDGEMENT

This work was conducted at the von Karman Gas Dynamics Facility at Arnold Engineering Development Center, Air Force Systems Command, Arnold Air Force Station, Tennessee.

The success of any program for the investigation of the turbulent wake behind hypersonic projectiles in an aeroballistic range is dependent on the efforts and activities of a large number of operating and support personnel. The authors express their appreciation to the members of the Aeroballistics Branch of VKF for the operation of the range and the acquiring of the data.

The authors wish to express their appreciation to Mr. Leith Potter for his advice and encouragement during this project and to the Air Force Systems Command for release of the data.

SYMBOLS

A	Cross-sectional area of body
a	Constant in mean value equation
b	Constant in mean value equation
C_D	Body drag coefficient
d	Diameter sphere or base *diameter of cone*
K	Correlation lag integer, $\xi = K\Delta X$
K_d	Kolmogoroff wave number
K_e	Energy containing wave number
l	Sample length
L_e	e-Fold correlation length

L_I	Integral correlation length
$\tilde{L}$	L_e or L_I
L_τ	Lagrangian integral time scale
M_∞	Body mach number
N	Total number of points sampled
N_o	Number of zero crossings of wake edge
N_{st}	Strouhal number
$P_f(y')$	Probability density
P_∞	Test section pressure
$Q_\epsilon(\xi)$	Auto-correlation function
$QC_{IJ}(\xi)$	Cross-correlation function
Re_∞	Body Reynolds number
RE(K)	Normalized auto-correlation function
$RC_{IJ}(\xi)$	Normalized cross-correlation function
Re_θ	$V_\infty \theta/\nu$
T_f	Static temperature at turbulent front
T_∞	Static temperature in test section
T_o	273°K
V_∞	Body velocity
V	Wake velocity at wake edge
X	Axial position in the wake
ΔX	Sample increment size
$\overline{X}$	Average vortex size at wake edge
Y	Coordinate in radial direction
Y_L	Coordinate in radial direction in lower profile
Y_u	Coordinate in radial direction in upper profile
Y_u'	Mean value of coordinate in radial direction in upper profile
$\overline{Y}$	Mean value of coordinate in radial direction
β	Wake front velocity / body velocity
ϵ	Deviation of wake edge position ($Y - \overline{Y}$)
ϵ_u	Deviation of upper wake edge position
η	x/d
λ	Microscale correlation length
λ_u	Upper profile microscale correlation length
ρ_∞	Test section density
ρ_o	1.29×10^{-3} gm/cm^3
σ_ϵ	Standard deviation of the wake edge position
σ_u	Standard deviation of the upper wake edge position
ϕ	Turbulence dissipation rate
ξ	Correlation lag distance
ν	Kinematic viscosity
ν_∞	Kinematic viscosity in test section
θ	$\sqrt{C_D A/2\pi}$
ω	Average wake width of sample

REFERENCES

1. Schapker, R. L., "Statistics of High-Speed Turbulent Wake Boundaries," AIAA J., 4, 1979-1987 (1966).
2. Levensteins, Z. J., and Krumins, M. V., "Aerodynamic Characteristics of Hypersonic Wakes," AIAA J., 5, 1596-1602 (1967).
3. Heckman, D., Tardif, L. and Lahaye, C., "Experimental Study of Turbulent Wakes in the CARDE Free-Flight Ranges," Proceedings of the Symposium on Turbulence of Fluids and Plasmas, Polytechnic Institute of Brooklyn, 1968.
4. Slattery, R. E., Clay, W. G., and Herrmann, J., "Gas and Electron Density Fluctuations in a Weakly Ionized Hypersonic Wake," Proceedings of the Symposium on Turbulence of Fluids and Plasmas, Polytechnic Institute of Brooklyn, 1968.
5. French, J. L., Personal Communication, VKF Gas Dynamics Facility, Aro, Inc., Arnold Air Force Station, Tennessee, 1968.
6. Fox, J. and Rungaldier, H., "Anemometer Measurements of Velocity and Density in Projectile Wakes," AIAA J., 9, 270 (1971).
7. Witte, A. B., Fox, J., Rungaldier, H., "Holographic Interferometry Measurements of Mean and Localized Fluctuating Wake Density Field for Cones Fired at Mach 6 in a Ballistic Range," presented at the AIAA 4th Fluid and Plasma Dynamics Conference, Palo Alto, California, June 21-23, 1971, Paper No. 71-564.
8. Clay, W. G., Herrmann, J., and Slattery, R. E., "Statistical Properties of the Turbulent Wake Behind Hypervelocity Spheres," Phys. Fluids, 8, 1792-1801 (1965).
9. Herrmann, J., Clay, W. G., Slattery, R. E., and Richardson, R. E., "Some Statistical Properties of Turbulent Wakes," Preprint of Fluid Physics of Hypersonic Wakes, AGARD - CP - No. 19, May 1967.
10. Uberoi, M. S., and Kovasznay, L. S. G., "Analysis of Turbulent Density Fluctuations by the Shadowgraph Method," J. Appl. Phys., 26, 19-24 (1955).
11. Zivanovic, S., Robillard, P. E., and Primich, R. I., "Radar Investigation of the Wakes of Blunt and Slender Hypersonic Velocity Projectiles in the Ballastic Range," Preprint Fluid Physics of Hypersonic Wakes, AGARD - CP - No. 19, May 1967.
12. Lane, F., "Frequency Effects in the Radar Return from Turbulent Weakly Ionized Missile Wakes," AIAA J., 5, 2193 (1967).
13. Schapker, R. L. and Camac, M., "NO_2 Chemiluminescent Wake Radiation," AIAA J., 7, 2254 (1969).
14. Reinecke, W. G., and McKay, W. L., "An Interferometric Study of the Turbulent Wake Behind a Hypersonic Sharp Slender Cone," AIAA J., 6, 1204 (1968).
15. Dionne, J. G. G., and Tardif, L., "Mean Density and Temperature Data In Wakes of Hypersonic Spheres," AIAA J., 8, 1707 (1970).
16. Bailey, A. B., Private communication, Arnold Engineering Development Center, Arnold Air Force Station, Tennessee.
17. Corrsin, S., and Kistler, A. L., "Free-stream Boundaries of Turbulent Flows," NACA Report No. 1244, 1955.
18. Demetriades, A., "Turbulent Fluctuation Measurements in Compressible Axisymmetric Wakes," AIAA J., 5, 1028-1029 (1967).
19. Fay, J. A., and Goldburg, A., "Unsteady Hypersonic Wake Behind Blunt Bodies," AIAA J., 1, 2264 (1963).
20. Goldburg, A., Washburn, W. K., and Florsheim, B. H., "Strouhal Numbers for the Hypersonic Wakes of Spheres and Cones," AMP-59 Avco Everett Research Laboratory Report, April 1965.